Synaptic vesicles undock and then transiently dock after an action potential

Grant F Kusick[1,2], Morven Chin[1°], Kristina Lippmann[3*#], Kadidia P Adula[3*†], M Wayne Davis[4], Erik M Jorgensen[3,4] & Shigeki Watanabe[1,3,5]

[1] Department of Cell Biology, Johns Hopkins University, School of Medicine, Baltimore, MD 21205, USA.
[2] Biochemistry, Cellular and Molecular Biology Graduate Program, Johns Hopkins University, School of Medicine, Baltimore, MD 21205, USA.
[3] Neurobiology Course, The Marine Biological Laboratory, Woods Hole, MA 02543, USA.
[4]Department of Biology and Howard Hughes Medical Institute, University of Utah, Salt Lake City, UT 84112-0840, USA.
[5]Solomon H. Snyder Department of Neuroscience, Johns Hopkins University, School of Medicine, Baltimore, MD 21205, USA.

[°] Current address: Program in Neuroscience, Harvard University, Cambridge, MA 02115, USA.
[#] Current address: Carl-Ludwig-Institute for Physiology, University Leipzig, 04103 Leipzig, Germany.
[†] Current address: Department of Molecular, Cell, and Developmental Biology, University of California, Los Angeles, Los Angeles, CA 90095, USA.
[*] These authors contributed equally to this work.

Correspondence:
Shigeki Watanabe (shigeki.watanabe@jhmi.edu)

Keywords
Synaptic vesicle exocytosis, neurotransmitter release, multivesicular release, asynchronous release, synaptic vesicle docking, transient docking, flash-and-freeze, zap-and-freeze

Abstract

Synaptic vesicles fuse with the plasma membrane to release neurotransmitter following an action potential, after which new vesicles must refill vacated release sites. How many vesicles can fuse at a single active zone, where they fuse within the active zone, and how quickly they are replaced with new vesicles is not well-established. To capture synaptic vesicle exocytosis at cultured mouse hippocampal synapses, we induced single action potentials by electrical field stimulation then subjected neurons to high-pressure freezing to examine their morphology by electron microscopy. During synchronous release, multiple vesicles can fuse at a single active zone; this multivesicular release is augmented by increasing the extracellular calcium concentration. Synchronous fusions are distributed throughout the active zone, whereas asynchronous fusions are biased toward the center of the active zone. Immediately after stimulation a large fraction of vesicles become undocked. Between 8 and 14 ms, new vesicles are recruited to the plasma membrane and fully replenish the docked pool, but docking of these vesicles is transient and they either undock or fuse within 100 ms. These results demonstrate that recruitment of synaptic vesicles to release sites is rapid and reversible.

When an action potential invades a synaptic bouton, voltage-gated calcium channels open and calcium influx triggers vesicle fusion to release neurotransmitter. Synaptic vesicle fusion takes place at a specialized membrane domain: the active zone[1]. It is believed that the active zone is organized into one or more release sites, which are individual units at which a single synaptic vesicle can fuse[2]. Ultrastructural studies demonstrate that some synaptic vesicles are in contact with the plasma membrane and define the 'docked' pool[3,4]. Since both docking and physiological readiness require engaged SNARE proteins[4–6], docked vesicles are thought to represent fusion-competent vesicles. There are several features of fusion that could be addressed by ultrastructural studies if methods existed to capture such rapid events as fusion and docking, specifically: how many vesicles fuse in response to an action potential, when and where they fuse, and how vesicle docking refills fusion sites.

How many vesicles fuse in response to an action potential has been intensely debated. A large body of work argues that, even when release probability is high, small central synapses act as binary operators: no more than one vesicle can fuse per action potential[7–10]. One possible mechanism is that the fusion of a vesicle blocks further fusions by 'lateral inhibition'[11,12]. By contrast, evidence from electrophysiology[13–16], optical imaging[17–21] and electron microscopy[22,23] suggests that multiple vesicles can fuse at a synapse[24].

Evoked neurotransmitter release takes place in two phases, with a synchronous component that begins within a millisecond of an action potential followed by an asynchronous component that can last for hundreds of milliseconds[25]. As opposed to the local calcium that triggers synchronous release, asynchronous release is triggered by the lower levels of residual calcium [25]. However, the mechanism for asynchronous fusion remains a mystery. Several high-affinity calcium sensors have been proposed to respond to this residual calcium and mediate asynchronous release[26,27]. Other proposed mechanisms include alternative sorting pathways for

asynchronous vesicles[28], an additional docking step in advance of asynchronous fusion[29], or a distinct location of the asynchronous pool relative to calcium channels [30,31]. Defining such a location by directly visualizing asynchronous release would resolve whether there is a specialized site of fusion for asynchronous release.

Docking of vesicles to refill release sites must be rapid. Even single action potentials can cause synaptic depression, but some central synapses can fire at a frequency of one kilohertz[32,33]. To avoid synaptic fatigue, active zones must quickly recruit vesicles from the cytoplasm. Yet recovery of the docked and readily-releasable vesicle pools is thought to be rather slow, on the order of a few seconds[23,34,35]. However, an emerging body of work suggests that vesicle replenishment constitutes several kinetically and molecularly distinct steps, some of which may occur on very fast timescales[36]. In two notable recent examples, modeling based on physiological data predicted that vesicles reversibly transition from "replacement sites" to "docking sites" within milliseconds of an action potential[29,37], and experiments with flash-and-freeze electron microscopy demonstrated that Synaptotagmin-1 mutants with docking defects can be reversed by binding calcium[38]. These fast vesicle docking events have been proposed to correspond to calcium-induced changes between loose and tight assembly of the SNARE complex, which may be both very fast and reversible[39]. However, there is currently no ultrastructural evidence for such fast and reversible docking steps at wild-type synapses.

To characterize the ultrastructure of vesicle fusion at active zones, we developed a method to trigger single action potentials by electrical stimulation followed by high-pressure freezing at defined time points called 'zap-and-freeze'. We observed that during synchronous release, multiple vesicles can fuse per action potential within the same active zone, even in physiological extracellular [Ca^{2+}]. Synchronous fusions occur throughout the active zone; however asynchronous fusions are concentrated at the active zone center. Unexpectedly, ~1/3 of

docked vesicles are lost immediately after stimulation, due not only to fusion but also to undocking. These are then fully replaced by newly docked vesicles within 14 ms, perhaps to counteract short-term depression. However, these vesicles are only transiently recruited and become undocked by 100 ms after stimulation. This sequence of rapid undocking, redocking, and subsequent slow undocking may underlie synaptic facilitation and depression.

Results

Zap-and-freeze captures synaptic vesicle fusion

To capture exocytosis with millisecond precision under physiologically-relevant conditions, we developed a system to electrically stimulate neurons before high-pressure freezing: a small, portable field-stimulation device with a photoelectric control switch (Fig. 1a). This device can be charged, then loaded into a high-pressure freezer and discharged with a flash of light to generate a 1 ms 10 V/cm stimulus before freezing at defined time points (see Methods).

To test whether this device is functional, we performed FM 1-43 loading experiments in mouse hippocampal neurons cultured on 6-mm sapphire disks. The lipophilic FM dye is taken up by compensatory endocytosis after synaptic vesicle fusion[40]. To prevent destaining by exocytosis, we applied Pitstop 2 (30 μM) 2 minutes prior to loading. Pitstop 2 is a nonspecific[41] but nonetheless potent inhibitor of clathrin-mediated vesicle formation[42]. The dye is taken up during ultrafast endocytosis, which is clathrin-independent, but will be trapped in synaptic endosomes which are resolved by clathrin-mediated budding[43]. Neurons were stimulated 10 times at 20 Hz, each pulse lasting 1 ms, which induces a single action potential. Following stimulation and fixation, presynaptic terminals throughout the sapphire disk were strongly labeled with FM 1-43 (Fig. 1b), suggesting that the electric field is fairly uniform across the surface of the 6-mm sapphire disk.

With the stimulation device validated, we next tested whether exocytic intermediates can be captured by high-pressure freezing. Experiments were performed at 37 °C and 1.2 mM external calcium, roughly the [Ca^{2+}] of the interstitial fluid in the brain[44]. Following a single 1 ms pulse, cells were frozen 5 ms after stimulation (Fig. 1c-d), which is the earliest possible time point given the mechanics of the high-pressure freezer (see Methods). Samples were then prepared for electron microscopy. In stimulated samples 18% of the synaptic profiles exhibited exocytic pits in the active zone (57/ 316), whereas in unstimulated cells only 2% of the synaptic profiles exhibited pits (6/ 275), and in cells in which action potentials were blocked by tetrodotoxin only 1% of the profiles contained pits (2/256) (Fig. 1e). Thus, the device induces *bona fide* action potentials and vesicle fusion, which can be reliably captured in electron micrographs. By analogy to the previously-developed flash-and-freeze[35], this technique is called 'zap-and-freeze'.

Multivesicular release is prominent in cultured hippocampal neurons

From single synaptic profiles, 2% (6/316 synaptic profiles) exhibited multiple pits. Although rare, the presence of multiple pits in the same image indicates that more than one vesicle in an active zone can fuse after a single action potential, an event known as multivesicular release[24]. However, the frequency of such events cannot be determined from single sections, but rather require reconstruction of whole active zones from serial sections (Fig. 2). To quantify synaptic vesicle fusions per synapse, we stimulated cultured neurons in 1.2 mM Ca^{2+} at 37 ºC and froze them 5 ms after stimulation, then reconstructed over 30 active zones for each condition and performed morphometry blinded (Extended Data Fig. 2a for example micrographs). In unstimulated samples, 3% of the synapses contained a pit (1/32), whereas in stimulated samples 27% of the synapses exhibited at least one pit (9/33, Fig. 2a). Of those with at

least 1 pit, 56% of active zones (5/9) contained multiple pits. All pits ranged from the size of a synaptic vesicle to expected sizes of vesicles at late stages of collapse into the plasma membrane (Fig. 2d; full range of pit widths at base, 34.6-70.6 nm). These results suggest that multivesicular release is prominent in cultured hippocampal neurons.

Multivesicular release is augmented by increasing extracellular calcium

Release probability is enhanced by increasing the extracellular calcium concentration[45]. To test the relationship between calcium concentration and vesicle fusion at individual active zones, we repeated the zap-and-freeze experiments in 2 mM and 4 mM calcium, since these concentrations have been frequently used to enhance fusion. Fusion was assessed by the presence of pits in the reconstructed active zones. Increasing the extracellular Ca^{2+} concentration did not change the fraction of synapses that responded (Fig. 2a): at all calcium concentrations only ~30% of active zones exhibited fusion pits (pits per active zone: 1.2 mM 27% 9/33; 2 mM 31% 11/36; 4 mM 27% 9/33; $p > 0.90$). However, increasing calcium did augment multivesicular release. In 1.2 mM Ca^{2+} 56% exhibited multivesicular release, in 2 mM Ca^{2+} 63% exhibited multivesicular release, and in 4 mM Ca^{2+} 89% exhibited multivesicular release, including one active zone with 5 pits. The presence of pits in ~30% of synapses at all calcium concentrations is consistent with the fraction of high-release probability terminals in hippocampal synapses[46–49], as well as potentially 'silent' synapses that never respond to stimulation[50].

In addition to the presence of pits, release could potentially be quantified as a decrease in docked vesicles due to full-collapse fusion[23,35,38]. Note that this calculation assumes that only docked vesicles can fuse after a single action potential, which is not necessarily true [29,37], and that vesicle undocking[51,52] is negligible. We counted the number of vesicles that were within 30 nm of the active zone membrane and classified those that were in physical contact with the

plasma membrane as docked. Docked vesicles were depleted after stimulation (Fig. 2c**)**. At 1.2 mM Ca^{2+}, the median number of docked vesicles decreased from 10 to 8 following stimulation ($p = 0.08$). At 2 mM Ca^{2+}, docked vesicles decreased from 14 to 11 at 2 mM ($p = 0.007$) and at 4 mM Ca^{2+} docked vesicles decreased from 12 to 7 ($p<0.001$). Although depletion of docked vesicles is consistent with vesicle fusion, loss of docked vesicles could also reflect undocking. Indeed, the number of docked vesicles also decreased at synapses that did not have pits (Fig. 2c). While it is possible that some fused vesicles had already fully collapsed and were missed, the profound decrease in docked vesicles could still only be explained by 1) a much higher proportion of synapses being active than indicated by the presence of pits, 2) nearly all of the vesicles fusing at those synapses that were active, which we did not observe for active zones that contained pits (Fig. 2c), or 3) docked vesicles being depleted by undocking in addition to loss from fusion. Therefore, these data suggest that, even in synapses that lack fusions, a fraction of docked vesicles undergo rapid undocking after stimulation.

Release sites within an active zone are independent

Recent studies suggest that many proteins essential for neurotransmitter release, including calcium channels, are clustered at the nanoscale, and these clusters seem to be distributed throughout the active zone[18,19,53,54]. To assess the distribution of release sites within active zones at the ultrastructural level, we mapped the locations of docked vesicles and exocytic pits (see Extended Data Fig. 3 for maps of pits and docked vesicles at all active zones that contained pits). Docked vesicles were found throughout the active zone without bias toward either the center or edge (with some exceptions, see Extended Data Table 1 for details; Fig. 2b). Vesicle fusions within the first 5 ms after an action potential were also distributed throughout the active zone (Fig. 2b**;** $p > 0.9$ for each). For each calcium concentration, the radial distribution of

pits and of docked vesicles in the active zone after stimulation were similar to those of docked vesicles from unstimulated controls (Fig. 2b**;** $p > 0.8$ for each). Thus, fusion competent vesicles are not enriched at either the center or periphery of the active zone.

However, fusion pits were occasionally found next to each other, suggesting that calcium influx from a single calcium channel or cluster of channels[55] may be responsible for multivesicular release. Unlike docked vesicles, the distances between pits were skewed toward shorter distances, suggesting that neighboring vesicles fuse simultaneously (Fig. 2e-f). Indeed, at 1.2 mM Ca^{2+} pits were usually within ~100 nm of each other (4 out of 5 multivesicular fusions). However, with increasing calcium concentrations, more distant fusion events (> 106 nm) were observed (Fig. 2f; 2 mM Ca^{2+}, 54% of fusion pits; 4 mM Ca^{2+}, 65% of fusion pits). Including data from all calcium concentrations (which is dominated by the large number of pits at 4 mM), the median distance between pits was not significantly different from that of docked vesicles (Fig. 2e, $p = 0.1$). Moreover, at 4 mM calcium the frequency of active zones with 1 to 5 pits matched a Poisson distribution (1 pit: 1 AZ; 2 pits: 3 AZ; 3 pits: 2 AZ; 4 pits: 2 AZ; 5 pits: 1 AZ) Thus, at high calcium concentrations, release sites act independently; that is, there is neither lateral inhibition[12] nor obvious coupling of release sites across an active zone. By contrast, at low calcium concentrations, adjacent vesicles tend to fuse together, possibly via a common calcium microdomain.

Synchronous and asynchronous fusion

To determine if vesicles continue to fuse after the 5 ms time point, we performed morphometry on synaptic profiles frozen 5, 8, 11, and 14 ms after an action potential (Fig. 3a-f, Extended Data Fig. 4a-b; 1.2 mM Ca^{2+}, 37 ºC). Pits peaked at 5 and 8 ms then declined to baseline by 14 ms (Fig. 3g; pits per profile: no stim 0.02, 5 ms 0.21, 8 ms 0.19, 11 ms 0.09, 14

ms 0.03; $p > 0.9$ compared to no stim). The depth of pits at 5 ms was variable (Fig. 3h; median = 16.2 nm, interquartile range: 13.2 to 22.7 nm), suggesting that some pits have collapsed by this time. Unexpectedly, pits at 11 ms were deeper than those at 5 ms (Fig. 3i; median at 5 ms 16.2 nm; at 11 ms 21.7 nm; $p = 0.05$). The presence of deep pits suggests that fusion of these vesicles may have initiated later, and may therefore represent asynchronous release[25].

To specifically test for asynchronous fusion, we assayed exocytosis in the presence of the slow calcium chelator EGTA-AM (25 μM). EGTA has a minor effect on synchronous release at most synapses[56] because the delay between calcium influx and vesicle fusion is less than a millisecond[57]. By contrast, it abolishes slower, asynchronous release[58]. In controls treated with DMSO, pits were apparent in active zone profiles at 5 and 11 ms (Fig. 4a; pits per synaptic profile: at 5 ms 0.16 pits; at 11 ms 0.17 pits; see Extended Data Fig. 5a for more micrographs). Treatment with 25 μM EGTA-AM had no effect at 5 ms, but eliminated fusion events at 11 ms (Fig. 4b-c; pits per synaptic profile: 5 ms 0.17 pits; 11 ms 0.04, pits, $p<0.001$; see Extended Data Fig. 5b for more micrographs). Thus, collapse of newly-fused vesicles must be rapid – less than 11 ms; the speed of collapse is thus faster than our previously calculated time constant of 20 ms[23]. These data demonstrate that fusion events observed at 5 and 11 ms represent synchronous and asynchronous release, respectively.

Asynchronous fusion at the center of the active zone

Two lines of evidence from 3D reconstructions suggest synchronous vesicle fusions are distributed evenly across the active zone. First, the distribution of pits 5 ms after stimulation matched the distribution of docked synaptic vesicles before stimulation (Fig. 2b). Second, the distribution of docked vesicles was not significantly altered after stimulation (Fig. 2b). This lack of bias was also observed in single profiles; pits and docked vesicles at 5 and 8 ms were not

biased toward the center or edge of the active zone (Fig. 3i, 4d, and Extended Data Fig. 4c; 5 ms and 8 ms, $p > 0.9$ in all cases). By contrast, pits at 11 ms and 14 ms were found near the center of the active zone more frequently (Fig. 3i, $p = 0.004$ and Fig. 4d, $p = 0.059$). Together, these data argue that vesicles fuse throughout the active zone during synchronous release, whereas asynchronous fusion occurs at the center of the active zone.

Vesicles undock then transiently dock after synchronous fusion

As synaptic vesicles are consumed during synchronous and asynchronous release, new vesicles must be recruited to the active zone. During synchronous fusion, docked vesicles were reduced by ~40% (Fig. 5a-b; docked vesicles per profile: no stim 1.6 vesicles; 5 ms 0.9 vesicles; 8 ms 1.0 vesicles; $p < 0.001$; see Fig. 2c for 3D analysis at 5 ms). During this time, the number of vesicles close to the membrane but not docked (between 6-10 nm) increased (Fig. 5c), possibly reflecting vesicles undocked from the active zone (Fig. 2c) or recruited from the cytoplasm. Such vesicles may provide a pool to replace those consumed by fusion. During asynchronous fusion, docked vesicles were not further depleted despite ongoing fusion, implying that synaptic vesicles are recruited during this process (Fig. 5a-b; 1.0 docked vesicles per synaptic profile; $p > 0.9$ vs 5 ms and 8 ms; $p < 0.001$ vs no stim). Strikingly, at 14 ms docked vesicles were fully restored to pre-stimulus levels (Fig. 5a-b; 1.4 docked vesicles per profile, $p > 0.9$ vs no stim). We previously observed that replenishment was slow: docked vesicles were depleted by 50 ms and returned to the baseline with a time constant of 3.8 s[23]. To address this apparent contradiction, we froze cells ~100 ms after an action potential. Docked vesicles were reduced by 30% at ~100 ms (Fig. 5d; docked vesicles per synaptic profile: no stim 1.8 vesicles; 105 ms 1.2 docked vesicles; $p < 0.001$), consistent with the previous study in which docked vesicles were reduced by ~40% at 100 ms[23]. Therefore, the

fast replenishment of docked vesicles observed at 14 ms is temporary. Such 'transient docking' could provide fusion-competent vesicles for asynchronous release[29] and counteract synaptic depression during trains of stimuli[38].

Discussion

We characterized docking and exocytosis of synaptic vesicles at hippocampal synapses in ultrastructural detail (Extended Data Fig. 1). Cultured neurons were subjected to a single stimulus, frozen at defined time points, and processed for electron microscopy. We performed morphometry on 3446 single synaptic profiles and 202 fully reconstructed active zones. Although ~70% of synapses do not respond to a single action potential, multivesicular release predominates in the 30% of synapses that respond to an action potential. Fusion sites are dispersed throughout the active zone, and vesicles fully collapse into the plasma membrane. Asynchronous fusion, defined as delayed events that are sensitive to the slow calcium buffer EGTA, occurs preferentially near the center of the active zone. By 14 ms, fused vesicles are fully replaced by new transiently docked vesicles, which return to the undocked state in less than 100 ms. These findings have implications for synaptic failure, multivesicular release, the spatial organization of release sites, and their refilling during short-term plasticity.

Roughly 70% of synapses in cultured hippocampal neurons do not respond to a single action potential. This failure rate is consistent with previous experiments in which we stimulated using channelrhodopsin rather than using electrical stimulation and assayed activity by endocytosis rather than by vesicle fusion[23,43]. This failure rate in itself is not unusual; the fraction of synapses that respond to a single action potential *in vivo* is low for many neurons of the central nervous system[59]. A 70% failure for individual synapses is consistent with the mean failure rate determined using a minimal stimulation protocol[49] or by use-dependent block of

NMDA glutamate receptors[46,47]. For example, in autaptic cultures 65% of synapses were found to have a low probability of release and 35% a high probability of release (C. Rosenmund, personal communication). Given that we stimulated only once, it is possible that all synapses have a uniform release probability of 0.30 and release is stochastic; that is, different synapses would be recruited with every stimulation. However, a large fraction of synapses in our cultures appear to be silent: First, increased calcium does not recruit more synapses: only ~30% of synapses exhibited vesicle fusion at 1.2 mM, 2 mM or 4 mM calcium. Second, in previous experiments, we used dynasore to block dynamin during multiple stimulations[39]. Only slightly more than 30% of the synapses exhibited trapped endocytic structures when stimulated 100 times. We conclude that most synapses in our cultures are not active even during high-frequency stimulation.

How many release sites are there within an active zone as determined by docking sites? The median number of docked vesicles in our experiments was ~10 per synapse (range 6-20, 1.2 mM calcium). Previous studies have observed means of 5-10 docked vesicles at hippocampal synapses[3,4,22,60,61]. The number of vesicles in the readily-releasable pool or the number of release sites at cultured hippocampal synapses determined using various fluorescence techniques was also 5-10[17,19,62,63]. Similarly, the number of Munc13 clusters, which is involved in docking and priming, was found to be 6[19] (range 0-17). Thus, the number of docked vesicles is similar to the number of release-ready vesicles.

The presence of multiple vesicles docked at a synapse alone does not imply that multiple vesicles can fuse at an active zone. In fact, it was long thought that only one vesicle could fuse in response to an action potential[10,24]. These studies argued that responses at synapses are mostly, or even exclusively, uniquantal, despite the presence of multiple docked vesicles. One mechanism put forward for univesicular release is that fusion of a vesicle can alter the active

zone by "lateral inhibition" and thereby block further fusions[11,12]. For proponents of univesicular release, examples of recordings of multivesicular events were dismissed as being caused by multiple active zones impinging on the cell. Proponents of multiquantal release at single active zones argued that observations of uniquantal events were due to saturation of the postsynaptic receptor field, and multiquantal release was observed under circumstances in which saturation could be avoided [13,14,15,16,20].

By reconstructing synapses immediately after a single action potential, we were able to directly capture multiple vesicles fusing in a single active zone. At 4 mM calcium, we observed up to 5 vesicles fusing in a single active zone. Moreover, the number of vesicles fusing at any particular active zone exhibited a Poisson distribution, suggesting that the release sites within an active zone were each behaving independently. The probability of fusion at a release site appears to be low even in elevated calcium ($p = \sim 0.15$ at 2 mM, ~0.25 at 4 mM), but because active zones have ~10 docking sites, synapses can consume multiple vesicles.

By contrast, at 1.2 mM calcium, fusions per synapse did not exhibit a Poisson distribution – more synapses exhibited two vesicles fusing than one. Importantly, fusing vesicles were adjacent to one another (< 100 nm). Adjacent fusions can also observed during spontaneous activity: In a previous study, 20% of synaptic profiles exhibiting spontaneous fusions comprised adjacent fusions, suggesting that fusing vesicles are coupled even in the absence of stimulation[22]. It is likely that coupled fusion is being driven by an active calcium channel or calcium microdomain that acts on locally docked vesicles[57,64].

In contrast to the microdomains that drive synchronous release, the residual calcium that triggers asynchronous release is more broadly distributed and longer-lasting[25,65]. This implies that there would be no spatial specificity for asynchronous fusion. However, we found that asynchronous release occurs at the center of the active zone, whereas synchronous fusion is

evenly distributed across the active zone. Several molecules, including VAMP4[66], Synaptotagmin-7[27], SNAP23[67] and Doc2[26], have been implicated in asynchronous release, and these molecules could target vesicles to release sites near the center of an active zone. Alternatively, the locations of voltage-gated calcium channel clusters within an active zone may account for this spatial arrangement. In both *Caenorhabditis elegans*[30] and *Drosophila melanogaster*[31] neuromuscular junctions, different isoforms of Unc13 position vesicles at different distances from the dense projection, where calcium channels reside[68]. Based on phenotypes from isoform-specific knockouts, these clusters were proposed to form independent release sites for fast and slow phases of neurotransmission.

A profound decrease in docking was observed after stimulation. Loss of docked vesicles via fusion can only account for ~30% of the decrease in docking. Moreover, docking is also reduced in synapses with no fusions. Therefore, we conclude that vesicles become undocked after a single action potential, likely caused by calcium influx. The loss of docked vesicles is accompanied by an increase in vesicles 6-10 nm from plasma membrane, suggesting that these vesicles may still be tethered to the membrane by a loosely assembled SNARE complex, synaptotagmin, or Munc13[4]. At 14 ms after the stimulation, docking levels are fully restored.

But then, by 100 ms docking is again reduced to the levels observed at 5 ms. Loss of docked vesicles at 100 ms is consistent with our previous results using optical stimulation[23]. Full and stable restoration of docking was not observed until 3-10 s[23] after stimulation, consistent with the recovery of the physiological readily-releasable pool[34]. Thus, there is a rapid undocking and redocking of vesicles after stimulation, but this docking is only transient.

What purpose could fast, ephemeral vesicle recruitment serve? Quite likely it is to maintain robust synaptic transmission during trains of stimuli. Recent electrophysiological studies of a cerebellar 'simple synapse' comprised of a single active zone indicate that a

population of vesicles may be undocked and occupy a 'replacement site'[29,37], possibly corresponding to our 10 nm pool. Based on modeling, vesicles in this pool are rapidly mobilized to dock at a release site, peaking ~10 ms after a stimulus. However, docked vesicles become undocked and return to the replacement site in the 100 ms following the action potential. Transient docking is likely mediated by the calcium sensor Synaptotagmin-1[38]. When Synaptotagmin-1's membrane-binding residues were mutated, vesicle docking was reduced by 30-50%. Docking was restored by a second action potential 10 ms after stimulation, but had declined after 100 ms, consistent with the time course of docking that we observed. Our data demonstrate that transient docking is not just a quirk of Synaptotagmin-1 mutants. Moreover, vesicles undock before transiently redocking.

In summary, we have characterized the ultrastructure of a synapse during the first 14 ms after an action potential using zap-and-freeze electron microscopy. At physiological calcium concentrations, an action potential typically drives multivesicular release from adjacent vesicles, likely via a shared calcium microdomain. It is presumed that such vesicles are docked to the membrane in a "tight-state" as recently proposed[39]. Stimulation is accompanied by a massive undocking of synaptic vesicles, nearly half at 4 mM calcium, even in synapses that do not exhibit fusion. We propose that calcium binding to Synaptotagmin-1, Munc13 or PIP2 drives docked vesicles into an undocked state. These undocked vesicles would still be associated with release sites but are tethered 10 nm from the membrane. Such vesicles are proposed to exist in a "loose-state" with SNAREs, Synaptotagmin-1, and Munc13 still engaged[69]. Between 8 and 14 ms, vesicles redock to the membrane, perhaps driven by calcium bound to Synaptotagmin-1 or the calcium sensor for facilitation, Synaptotagmin-7[70]. Redocking is occurring at the same time as vesicles are undergoing asynchronous fusion and may perhaps represent vesicles undergoing '2-step' release[29]. Docking levels are fully restored 14 ms after stimulation; however, this docking

is not stable, and declines along with falling calcium levels. Thereafter full docking is not restored until 3-10 seconds later. Thus, synaptic vesicles at the active zone exhibit surprisingly lively dynamics between docked and undocked states within milliseconds after an action potential.

References

1. Heuser, J. E. *et al.* Synaptic vesicle exocytosis captured by quick freezing and correlated with quantal transmitter release. *J. Cell Biol.* **81,** 275–300 (1979).
2. Kaeser, P. S. & Regehr, W. G. The readily releasable pool of synaptic vesicles. *Curr. Opin. Neurobiol.* **43,** 63–70 (2017).
3. Schikorski, T. & Stevens, C. F. Quantitative ultrastructural analysis of hippocampal excitatory synapses. *J. Neurosci.* **17,** 5858–5867 (1997).
4. Imig, C. *et al.* The Morphological and Molecular Nature of Synaptic Vesicle Priming at Presynaptic Active Zones. *Neuron* **84,** 416–431 (2014).
5. Hammarlund, M., Palfreyman, M. T., Watanabe, S., Olsen, S. & Jorgensen, E. M. Open syntaxin docks synaptic vesicles. *PLoS Biol.* **5,** 1695–1711 (2007).
6. Richmond, J. E., Weimer, R. M. & Jorgensen, E. M. An open form of syntaxin bypasses the requirement for UNC-13 in vesicle priming. *Nature* **412,** 338–341 (2001).
7. Korn, H., Triller, A., Mallet, A. & Faber, D. S. Fluctuating responses at a central synapse: n of binomial fit predicts number of stained presynaptic boutons. *Science (80-.).* **213,** 898–901 (1981).
8. Redman, S. & Walmsley, B. Amplitude fluctuations in synaptic potentials evoked in cat spinal motoneurones at identified group Ia synapses. *J. Physiol.* **343,** 135–145 (1983).
9. Gulyás, a I. *et al.* Hippocampal pyramidal cells excite inhibitory neurons through a single release site. *Nature* **366,** 683–687 (1993).
10. Redman, S. Quantal analysis of synaptic potentials in neurons of the central nervous system. *Physiol. Rev.* **70,** 165–198 (1990).
11. Stevens, C. F. & Wang, Y. Facilitation and depression at single central synapses. *Neuron* **14,** 795–802 (1995).
12. Dobrunz, L. E., Huang, E. P. & Stevens, C. F. Very short-term plasticity in hippocampal

synapses. *Proc. Natl. Acad. Sci.* **94,** 14843–14847 (1997).

13. Tong, G. & Jahr, C. E. Multivesicular release from excitatory synapses of cultured hippocampal neurons. *Neuron* **12,** 51–59 (1994).
14. Auger, C., Kondo, S. & Marty, A. Multivesicular Release at Single Functional Synaptic Sites in Cerebellar Stellate and Basket Cells. *J. Neurosci.* **18,** 4532–4547 (1998).
15. Christie, J. M. & Jahr, C. E. Multivesicular Release at Schaffer Collateral-CA1 Hippocampal Synapses. *J. Neurosci.* **26,** 210–216 (2006).
16. Malagon, G., Miki, T., Llano, I., Neher, E. & Marty, a. Counting vesicular release events reveals binomial release statistics at single glutamatergic synapses. *J. Neurosci.* **36,** 4010–4025 (2016).
17. Maschi, D. & Klyachko, V. A. Spatiotemporal Regulation of Synaptic Vesicle Fusion Sites in Central Synapses. *Neuron* 1–9 (2017). doi:10.1016/j.neuron.2017.03.006
18. Tang, A.-H. *et al.* A trans-synaptic nanocolumn aligns neurotransmitter release to receptors. *Nature* **536,** 210–214 (2016).
19. Sakamoto, H. *et al.* Synaptic weight set by Munc13-1 supramolecular assemblies. *Nature Neuroscience* **21,** 41–55 (2018).
20. Conti, R. & Lisman, J. The high variance of AMPA receptor- and NMDA receptor-mediated responses at single hippocampal synapses: Evidence for multiquantal release. *Proc. Natl. Acad. Sci.* **100,** 4885–4890 (2003).
21. Balaji, J. & Ryan, T. A. Single-vesicle imaging reveals that synaptic vesicle exocytosis and endocytosis are coupled by a single stochastic mode. *Proc. Natl. Acad. Sci.* **104,** 20576–20581 (2007).
22. Abenavoli, A. *et al.* Multimodal quantal release at individual hippocampal synapses: evidence for no lateral inhibition. *J. Neurosci.* **22,** 6336–46 (2002).

23. Watanabe, S. *et al.* Ultrafast endocytosis at mouse hippocampal synapses. *Nature* **504,** 242–7 (2013).

24. Rudolph, S., Tsai, M.-C., von Gersdorff, H. & Wadiche, J. I. The ubiquitous nature of multivesicular release. *Trends Neurosci.* **38,** 428–438 (2015).

25. Kaeser, P. S. & Regehr, W. G. Molecular mechanisms for synchronous, asynchronous, and spontaneous neurotransmitter release. *Annu. Rev. Physiol.* **76,** 333–63 (2014).

26. Yao, J., Gaffaney, J. D., Kwon, S. E. & Chapman, E. R. Doc2 is a Ca 2+ sensor required for asynchronous neurotransmitter release. *Cell* **147,** 666–677 (2011).

27. Turecek, J. & Regehr, X. W. G. Synaptotagmin 7 Mediates Both Facilitation and Asynchronous Release at Granule Cell Synapses. *J. Neurosci.* **38,** 3240–3251 (2018).

28. Evstratova, A., Chamberland, S., Faundez, V. & To, K. Vesicles derived via AP-3-dependent recycling contribute to asynchronous release and influence information transfer. *Nat. Commun.* (2014). doi:10.1038/ncomms6530

29. Miki, T., Nakamura, Y., Malagon, G., Neher, E. & Marty, A. Two-component latency distributions indicate two-step vesicular release at simple glutamatergic synapses. *Nat. Commun.* **9,** 3943 (2018).

30. Hu, Z., Tong, X. J. & Kaplan, J. M. UNC-13L, UNC-13S, and Tomosyn form a protein code for fast and slow neurotransmitter release in Caenorhabditis elegans. *Elife* **2013,** 1–20 (2013).

31. Böhme, M. A. *et al.* Active zone scaffolds differentially accumulate Unc13 isoforms to tune Ca(2+) channel-vesicle coupling. *Nat. Neurosci.* **19,** (2016).

32. Delvendahl, I. & Hallermann, S. The Cerebellar Mossy Fiber Synapse as a Model for High-Frequency Transmission in the Mammalian CNS. *Trends Neurosci.* **39,** 722–737 (2016).

33. Ritzau-jost, A. *et al.* Ultrafast Action Potentials Mediate Kilohertz Signaling at a Central Synapse. *Neuron* **84,** 152–163 (2014).

34. Pyott, S. J. & Rosenmund, C. The effects of temperature on vesicular supply and release in autaptic cultures of rat and mouse hippocampal neurons. *J. Physiol.* **539,** 523–535 (2002).

35. Watanabe, S. *et al.* Ultrafast endocytosis at Caenorhabditis elegans neuromuscular junctions. *Elife* **2013,** e00723 (2013).

36. Hallermann, S. Looking into the Black Box of Synaptic Vesicle Recruitment. *Neuron* **88,** 435–437 (2015).

37. Miki, T. *et al.* Actin- and Myosin-Dependent Vesicle Loading of Presynaptic Docking Sites Prior to Exocytosis. *Neuron* **91,** 808–823 (2016).

38. Chang, S., Trimbuch, T. & Rosenmund, C. Synaptotagmin-1 drives synchronous Ca2+-triggered fusion by C2B-domain-mediated synaptic-vesicle-membrane attachment. *Nat. Neurosci.* **21,** 33–42 (2018).

39. Neher, E. & Brose, N. Dynamically Primed Synaptic Vesicle States: Key to Understand Synaptic Short-Term Plasticity. *Neuron* **100,** 1283–1291 (2018).

40. Betz, W. J. & Bewick, G. S. Optical analysis of synaptic vesicle recycling at the frog neuromuscular junction. *Science (80-.).* **255,** 200–203 (1992).

41. Dutta, D., Williamson, C. D., Cole, N. B. & Donaldson, J. G. Pitstop 2 Is a Potent Inhibitor of Clathrin-Independent Endocytosis. *PLoS One* **7,** 1–9 (2012).

42. Von Kleist, L. *et al.* Role of the clathrin terminal domain in regulating coated pit dynamics revealed by small molecule inhibition. *Cell* **146,** 471–484 (2011).

43. Watanabe, S. *et al.* Clathrin regenerates synaptic vesicles from endosomes. *Nature* **515,** 228–33 (2014).

44. Jones, H. C. & Keep, R. F. Brain fluid calcium concentration and response to acute hypercalcaemia during development in the rat. *J. Physiol.* **402,** 579–593 (1988).

45. Katz, B. & Miledi, R. The effect of calcium on acetylcholine release from motor nerve terminals. *Proc. R. Soc. B Biol. Sci.* **161,** 496–503 (1965).

46. Rosenmund, C., Clements, J. D. & Westbrook, G. L. Nonuniform Probability of Glutamate Release at a Hippocampal Synapse. *Science (80-.).* **262,** 754–757 (1993).

47. Hessler, N. A., Shirke, A. M. & Malinow, R. The probability of transmitter release at a mammalian central synapse. *Nature* **366,** 569–572 (1993).

48. Murthy, V. N., Sejnowski, T. J. & Stevens, C. F. Heterogeneous release properties of visualized individual hippocampal synapses. *Neuron* **18,** 599–612 (1997).

49. Allen, C. & Stevens, C. F. An evaluation of causes for unreliability of synaptic transmission. *Proc. Natl. Acad. Sci. U. S. A.* **91,** 10380–3 (1994).

50. Yao, J., Qi, J. & Chen, G. Actin-Dependent Activation of Presynaptic Silent Synapses Contributes to Long-Term Synaptic Plasticity in Developing Hippocampal Neurons. *J. Neurosci.* **26,** 8137–8147 (2006).

51. Murthy, V. N. & Stevens, C. F. Reversal of synaptic vesicle docking at central synapses. *Nat. Neurosci.* **2,** 503–507 (1999).

52. Zenisek, D., Steyer, J. A. & Almers, W. Transport , capture and exocytosis of single synaptic vesicles at active zones. *Nature* **406,** 849–854 (2000).

53. Ehmann, N., Sauer, M. & Kittel, R. J. Super-resolution microscopy of the synaptic active zone. *Front. Cell. Neurosci.* **9,** 7 (2015).

54. Hruska, M., Henderson, N., Le Marchand, S. J., Jafri, H. & Dalva, M. B. Synaptic nanomodules underlie the organization and plasticity of spine synapses. *Nat. Neurosci.* **21,** 671–682 (2018).

55. Miki, T. *et al.* Numbers of presynaptic Ca $^{2+}$ channel clusters match those of functionally defined vesicular docking sites in single central synapses. *Proc. Natl. Acad. Sci.* 201704470 (2017). doi:10.1073/pnas.1704470114

56. Grauel, M. K. *et al.* RIM-binding protein 2 regulates release probability by fine-tuning calcium channel localization at murine hippocampal synapses. *Proc. Natl. Acad. Sci.* **113,** 11615–11620 (2016).

57. Adler, E., Augustine, J., Duffy, N. & Charlton, P. Alien Intracellular Calcium Chelators Attenuate Release at the Squid Giant Synapse. *J. Neurosci.* **11,** 1496–1507 (1991).

58. Chen, C. & Regehr, W. G. Contributions of residual calcium to fast synaptic transmission. *J. Neurosci.* **19,** 6257–66 (1999).

59. Borst, J. G. G. The low synaptic release probability in vivo. *Trends Neurosci.* **33,** 259–266 (2010).

60. Holderith, N. *et al.* Release probability of hippocampal glutamatergic terminals scales with the size of the active zone. *Nat. Neurosci.* **15,** 988–97 (2012).

61. Harris, K. M. & Sultan, P. Variation in the Number , Location and Size of Synaptic Vesicles Provides an Anatomical Basis for the Nonuniform Probability of Release at Hippocampal CA1 Synapses. *Neuropharmacology* **34,** 1387–1395 (1995).

62. Murthy, V. N., Schikorski, T., Stevens, C. F., Zhu, Y. & Jolla, L. Inactivity produces increases in neurotransmitter release and synaptic size. *Neuron* **32,** 673–682 (2001).

63. Ariel, P. & Ryan, T. A. Optical mapping of release properties in synapses. *Front. Neural Circuts* **4,** (2010).

64. Nakamura, Y. *et al.* Nanoscale Distribution of Presynaptic Ca2+ Channels and Its Impact on Vesicular Release during Development. *Neuron* **85,** 145–159 (2015).

65. Sabatini, B. L. & Regehr, W. G. Optical measurement of presynaptic calcium currents.

Biophys. J. **74,** 1549–1563 (1998).

66. Raingo, J. *et al.* VAMP4 directs synaptic vesicles to a pool that selectively maintains asynchronous neurotransmission. *Nat. Neurosci.* **15,** 738–745 (2012).

67. Weber, J. P., Toft-Bertelsen, T. L., Mohrmann, R., Delgado-Martinez, I. & Sørensen, J. B. Synaptotagmin-7 is an asynchronous calcium sensor for synaptic transmission in neurons expressing SNAP-23. *PLoS One* **9,** 1–22 (2014).

68. Clustering, C. C. *et al.* Bruchpilot Promotes Active Zone Assembly, Ca2+ Channel Clustering, and Vesicle Release. *Science (80-.).* **312,** 1051–1054 (2006).

69. Lipstein, N. *et al.* Dynamic Control of Synaptic Vesicle Replenishment and Short-Term Plasticity by Ca2+-Calmodulin-Munc13-1 Signaling. *Neuron* **79,** 82–96 (2013).

70. Jackman, S. L., Turecek, J., Belinsky, J. E. & Regehr, W. G. The calcium sensor synaptotagmin 7 is required for synaptic facilitation. *Nature* **529,** 88–91 (2016).

71. Kaech, S. & Banker, G. Culturing hippocampal neurons. *Nat. Protoc.* **1,** 2406–2415 (2006).

72. Hoopmann, P., Rizzoli, S. O. & Betz, W. J. Imaging synaptic vesicle recycling by staining and destaining vesicles with FM dyes. *Cold Spring Harb. Protoc.* **7,** 77–83 (2012).

73. Hoppa, M. B., Gouzer, G., Armbruster, M. & Ryan, T. A. Control and plasticity of the presynaptic action potential waveform at small CNS nerve terminals. *Neuron* **84,** 778–789 (2014).

74. Watanabe, S. Flash-and-Freeze: Coordinating Optogenetic Stimulation with Rapid Freezing to Visualize Membrane Dynamics at Synapses with Millisecond Resolution. *Front. Synaptic Neurosci.* **8,** 24 (2016).

Methods

All animal care was performed according to the National Institutes of Health guidelines for animal research with approval from the Animal Care and Use Committee at the Johns Hopkins University School of Medicine.

Neuronal cell culture

Cell cultures were prepared on 6-mm sapphire disks (Technotrade), mostly as previously described[23,43]. Newborn or embryonic day 18 C57/BL6J mice of both sexes were decapitated, followed by dissection of and transfer of brains to ice-cold HBSS. In the case of embryonic mice, heads were stored in HBSS on ice prior to dissection. For high-pressure freezing, neurons were cultured on a feeder layer of astrocytes. For FM dye experiments, astrocytes were grown on 22-mm coverslips for 1 week and placed on top of neurons cultured on sapphire disks with astrocytes facing neurons[71], with Paraffin dots used as spacers. Astrocyte cultures were established from cortices trypsinized for 20 min at 37 °C with shaking, followed by trituration and seeding on T-75 flasks. Astrocytes were grown in DMEM supplemented with 10% FBS and 0.1% penicillin-streptomycin for 2 weeks, then plated on PDL-coated 6mm sapphire disks atop glass coverslips in 12-well plates at a density of 50,000/well to create a feeder layer. After six days, FUDR was added to stop cell division. The following morning, culture medium was replaced with Neurobasal-A supplemented with 2% B27 and 0.1% penicillin-streptomycin (NB-A full medium, Invitrogen) prior to plating hippocampal neurons. Hippocampi were dissected and incubated in papain with shaking at 37 °C for 30-60 min, then triturated and plated on astrocytes at 50,000 or 75,000 cells/well. Before use, sapphire disks were carbon-coated with a “4” to indicate the side that cells are cultured on. Health of the cells, as indicated by de-adhered processes, floating dead cells, and excessive clumping of cell bodies, was assessed regularly, as well as immediately before experiments. All experiments were performed between 13 and 17 days *in vitro*.

Electrical field stimulation

The electrical stimulator is manufactured by Leica to be compatible with the Leica ICE high pressure freezer. The middle plate was designed as a circuit board trimmed to the dimensions of a standard Leica ICE high-pressure freezer middle plate. In the middle plate, there is a central 6 mm hole holding the sample sandwiched between two sapphire disks. This central hole was plated with two gold contact surfaces that are used to apply field stimulation to the sample. The standard spacer ring between the sapphire disks are conductive, and is replaced with nonconductive mylar rings of the same dimensions. The voltage to be applied to the sample is provided by a capacitor bank attached to the middle plate. The capacitors are charged just before the sample is loaded into the chamber. The current from the capacitors to the sample is controlled by a phototransistor. In the absence of light, there is no current passed from the capacitors to the sample contacts. In this way, the field stimulation can be activated within the chamber using the standard light stimulation function of the EM ICE.

FM dye uptake imaging

For the FM 1-43FX (Invitrogen) uptake assay, we used a modified version of a previously published protocol[72]. Neurons on sapphire disks were first incubated with 30 µM Pitstop 2 (Sigma) in physiological saline (1 mM Ca^{2+}) for 2 min. This treatment blocks regeneration of synaptic vesicles from synaptic endosomes[43], so as to prevent FM dyes from being released during the washing procedure. Following addition of FM dye (5 µg/ml), a sapphire disk was mounted on a middle plate, while another sapphire disk in the same well was left in the solution to ensure that both sapphire disks were incubated in FM dye for the same period of time. After charging the middle plate, 10 pulses of light (1 ms each) were applied at 20 Hz to discharge the capacitor and induce 10 action potentials. Immediately after stimulation, both stimulated and unstimulated specimens were transferred to an 18-mm petri

dish containing physiological saline solution (1 mM Ca^{2+}). FM dyes bound to the plasma membrane were washed off by passing current across the specimen using a transfer pipet for 1 min. Both samples were then transferred into warm (37 ºC) PBS containing 4% paraformaldehyde and fixed for 30 min. After fixation, samples were washed 3x with PBS and immediately imaged on an Olympus IX81 epifluorescence microscope equipped with a Hamamatsu C9100-02 EMCCD camera with mercury lamp illumination through a CFP/YFP filter set (Semrock) and a 60x, NA 1.4 Olympus UIS2 oil-immersion objective. All micrographs shown were acquired with the same settings on the microscope and later adjusted in brightness and contrast to the same degree in ImageJ, then rotated and cropped in Adobe Photoshop.

High-pressure freezing

Cells cultured on sapphire disks were frozen using an EM ICE high-pressure freezer (Leica Microsystems). The freezing apparatus was assembled on a table heated to 37 °C in a climate control box, with all solutions pre-warmed (37 ºC). Sapphire disks with neurons were carefully transferred from culture medium to a small culture dish containing physiological saline solution (140 mM NaCl, 2.4 mM KCl, 10 mM HEPES, 10 mM glucose; pH adjusted to 7.3 with NaOH, 300 mOsm). NBQX (3 μM; Tocris) and bicuculline (30 μM; Tocris) were added to the physiological saline solution to block recurrent synaptic activity. $CaCl_2$ and $MgCl_2$ concentrations were 1.2 mM and 3.8 mM, respectively, except where indicated, in which case the $MgCl_2$ concentration was adjusted accordingly (3 mM $MgCl_2$ with 2 mM $CaCl_2$, 1 mM $MgCl_2$ with 4 mM $CaCl_2$). Cells were then fitted into the photoelectric middle plate. Filter paper was placed underneath the middle plate to remove all excess liquid. A mylar spacer ring was then placed atop the sapphire disk. To create a “sandwich” of the solution described above, the underside of another sapphire disk was dipped in the solution so

that some was held on by surface tension, then placed atop the spacer ring so that excess liquid again dispersed onto the filter paper. For voltage to be applied across the sample, it is essential for all components outside of the sandwich to be dry, so the top of the sapphire and all other components of the setup were gently dried with another piece of filter paper. Finally, a rubber ring was added to hold everything in place. This entire assembly process takes 3-5 min. The assembled middle plate was enclosed in two half cylinders then loaded into the freezing chamber, where the cells were stimulated for 1 ms before freezing at the desired time point, ranging from 5 ms to 105 ms. With this protocol, 10 V/cm is applied for 1 ms across a 6-mm space between the electrodes into which the sapphire disk fits, as confirmed by measurements from Leica. This field stimulation regimen in hippocampal cultures induces a single action potential and only negligibly depolarizes boutons directly[73].

For EGTA experiments, first half of the media in which cells were grown was removed and set aside. EGTA-AM (Fisher) or DMSO was then added to media to a final concentration of 25 μM and 0.25% DMSO for 15 min to load the cells with EGTA. Cells were washed three times and left in the media that had been set aside for 15 min before freezing in the physiological saline solution described above (treatment protocol adapted from [56]). For TTX experiments, TTX was added to the freezing solution to a final concentration of 1 μM, such that cells were in TTX for 3-5 min before freezing.

Cooling rates during freezing were between 16,000-18,000 K/sec, and pressure reached 2,250 bar within 10 ms. Membrane traffic stops at 0 °C, so the point at which the sample reaches this temperature can be considered the true time of freezing. Previous experiments indicated that the temperature sensor placed immediately before the sample reaches 0 °C 2.2 ± 0.08 ms from the onset of freezing in the EM ICE, with a full range of 1.5-3.5 ms[74]. Based on previous estimates[23], the sample is expected to reach the same temperature

after another 3 ms. Therefore, specimens were frozen, on average, 5 ms later than the time point programmed into the EM ICE, with relatively little variability (for example, to freeze at 5 ms, the delay period on the machine was set to "0 ms"). The time points indicated (5, 8, 11, 14, and 105 ms) are calculated based on this estimated 5 ms delay from the onset of stimulation.

Freeze-substitution

After freezing, samples were transferred under liquid nitrogen to an EM AFS2 freeze substitution system at -90 °C (Leica Microsystems). Using pre-cooled tweezers, samples were quickly transferred to anhydrous acetone at -90 °C. After disassembling the freezing apparatus, sapphire disks with cells were quickly moved to cryovials containing 1% glutaraldehyde, 1% osmium tetroxide, and 1% water in anhydrous acetone, which had been stored under liquid nitrogen then moved to the AFS2 immediately before use. The freeze substitution program was as follows: −90 °C for 6-10 hr (adjusted so substitution would finish in the morning), 5 °C h^{-1} to −20 °C, 12 h at -20 °C, and 10 °C h^{-1} to 20 °C.

Embedding, sectioning, and transmission electron microscopy

Samples in fixatives were washed three times, 10 min each, with anhydrous acetone, then stained *en bloc* with 1% uranyl acetate for 1 hr with shaking. After three washes, samples were left in 30% epon araldite in anhydrous acetone for 3 hr, then 70% epon araldite for 2 hr, both with shaking. Samples were then transferred to caps of polyethylene BEEM capsules (EMS) and left in 90% epon araldite overnight at 4 °C. The next morning, samples were transferred to 100% epon araldite (epon, 6.2 g; araldite, 4.4 g; DDSA, 12.2 g; and BDMA, 0.8 ml) for 1 hr, then again to 100% for 1 hr, and finally transferred to 100% epon araldite and baked at 60 °C for 48 hr.

For single-section imaging, 40-nm sections were cut, while 8-10 50-nm sections were cut for serial-section 3D reconstructions. Sections on single-slot grids coated with 0.7% pioloform were stained with 2.5% uranyl acetate then imaged at 80 kV on the 93,000x setting on a Phillips CM 120 transmission electron microscope equipped with an AMT XR80 camera. In some cases, including all serial-section imaging, the microscopist was blind to the different conditions, while in other cases they were not. To limit bias, synapses were found by bidirectional raster scanning along the section at 93,000x, which makes it difficult to "pick" certain synapses, as a synapse usually takes up most of this field of view. Synapses were identified by a vesicle-filled presynaptic bouton and a postsynaptic density. Postsynaptic densities are often subtle in our samples, but synaptic clefts were also identifiable by 1) their characteristic width, 2) the apposed membranes following each other closely, and 3) vesicles near the presynaptic active zone. Only synapses with prominent post-synaptic densities were imaged for serial-sectioning reconstructions. 125-150 Micrographs per sample of anything that appeared to be a synapse were taken without close examination. For serial sectioning, at least 30 synapses per sample were imaged.

Electron microscopy image analysis

For single-section analysis, images were annotated blind but not randomized in the initial time course experiments (first replicate of data shown in Figure 3). For all other single-section data, all the images from a single experiment were randomized for analysis as a single pool using a custom R (R Development Team) script. Only after this randomization were images excluded from analysis, either because they appeared to not contain a *bona fide* synapse or the morphology was too poor for reliable annotation. This usually meant ~100 synapses per sample were analyzed. Serial section images were not randomized, but the

observer was always blind to the sample conditions. The plasma membrane, active zone, docked synaptic vesicles, synaptic vesicles close to the active zone, and pits (putative fusion events) were annotated in ImageJ using a custom plugin. The active zone was identified as the region of the presynaptic plasma membrane with the features described above for identifying a synapse. Docked vesicles were identified by their membrane appearing to be in contact with the plasma membrane at the active zone. Vesicles that were not manually annotated as docked, but were 0 nm away from the active zone plasma membrane, were automatically counted as docked when segmentation was quantitated (see below) for data sets counting the number of docked vesicles, but were not included in data sets mapping the locations of docked vesicles. Pits were identified as smooth curvature (not mirrored by the postsynaptic membrane) in an otherwise straight membrane. All image segmentation, still in the form of randomized files, was thoroughly checked by a second member of the lab. Features were then quantitated using custom MATLAB (MathWorks) scripts.

Location of pits and docked vesicles within the active zone from single sections was calculated from the distance from the center of the pit to the center and the edge of the active zone in 2D. Distance from the center was normalized by dividing the distance to the edge by the half-width of the active zone. For 3D data, the distance to the center of the active zone was calculated from serial sections. First, the location in 2D was calculated as above. Then, the 3D distance was calculated to the center of the active zone in the middle section of the series using the Pythagorean theorem with assumption that each section is 50 nm thick. Locations in 3D data were further corrected to be the density of vesicles/pits at each distance from the center of the active zone. This is because the total area for objects to be located in increases with increasing distance from the center of a roughly circular object (for example, randomly distributed objects within a circular active zone would have a median distance from

the center of 0.66, giving the impression that they are biased toward the edge: after calculating the density, this value would be 0.5). To calculate density of vesicles/pits from the center to the edge in 3D reconstructions, the radial position of each vesicle/pit was converted to the fractional area of a circle bounded by that radius. In the case of a unit circle (distance from center to edge is by definition 1 data normalized to the size of the active zone), this is simply the square of the original normalized distance to the center. Distance between pits and docked vesicles in different sections was approximated in a similar manner, where the edges of the hypothetical triangle are 1) the difference of the distances between each pit to the center of the active zone in each section and 2) the distance between the sections, again assuming a thickness of 50 nm.

Example micrographs shown were adjusted in brightness and contrast to different degrees (depending on the varying brightness and contrast of the raw images), rotated, and cropped in Adobe Photoshop.

Statistical analysis

All data are from two different experiments from two separate cultures, except for data from serial section 3D reconstructions and the TTX-treated sample without stimulation, which are from single experiments, and data from untreated cells frozen at 5 ms and 8 ms after stimulation, which are from three experiments. Images from the FM dye uptake assay are from one experiment. Data from the two experiments were pooled for statistical analysis. We did not predetermine sample sizes using power analysis, but based them (N=2, n≈200) on our prior experience with flash-and-freeze data[23,35,43]. An alpha of 0.05 was used for statistical hypothesis testing. All data were tested for normality by D'Agostino-Pearson omnibus test to determine whether parametric or nonparametric methods should be used. Comparisons

between two groups were performed using a Welch two-sample t-test or Wilcoxon rank-sum test. Comparisons between multiple groups followed by full pairwise comparisons were performed using one-way analysis of variance (ANOVA) followed by Tukey's HSD test or Kruskal-Wallis test followed by Dunn's multiple comparisons test. Differences in the number of active zones containing at least one pit from active zone reconstructions in Figure 2a were assessed using a chi-square test. For testing whether locations of pits were biased toward the center or edge of the active zone, a one-sample t-test or Wilcoxon rank-sum test with a theoretical median of 0.5 was used (each of these p-values, as well as that of the comparisons between pit locations in different samples, were accordingly corrected for multiplicity using Bonferroni's method). All statistical analyses were performed and all graphs created in Graphpad Prism 7.

Life Sciences Reporting Summary

More details on experimental procedures, materials, and statistics are available in the Life Sciences Reporting Summary.

Data and code availability.

The data underlying this work, as well as custom R and MATLAB scripts, are available upon request.

Acknowledgements

We are indebted to Sumana Raychaudhuri, Shuo Li, and Quan Gan for cell culture, help with freezing, and stimulating discussions. We also thank Mike Delanoy and Barbara Smith for technical assistance with electron microscopy and Kathleen T DiNapoli for developing R code to randomize images. We thank Paul Wurzinger and Cveta Tomova at Leica for design and

manufacture of middle plate. S.W. and this work were supported by start-up funds from the Johns Hopkins University School of Medicine, Johns Hopkins Discovery funds, and the National Science Foundation (1727260), the National Institute of Health (1DP2 NS111133-01 and 1R01 NS105810-01A1) awarded to S.W. S.W. is an Alfred P. Sloan fellow. EMJ is an Investigator of the Howard Hughes Medical Institute. G.F.K. was supported by a grant from the National Institutes of Health to the Biochemistry, Cellular and Molecular Biology program of the Johns Hopkins University School of Medicine (T32 GM007445) and is a National Science Foundation Graduate Research Fellow (2016217537). The EM ICE high-pressure freezer was purchased partly with funds from an equipment grant from the National Institutes of Health (S10RR026445) awarded to Scot C Kuo.

Author Contributions

M.W.D., S.W., and E.M.J. conceived the zap-and-freeze technique. G.F.K. and S.W. designed the experiments and analyzed the data. S.W., G.F.K., and E.M.J wrote the manuscript. G.F.K. performed all freezing experiments and single-section electron microscopy sample preparation, imaging, and analysis, and FM dye uptake experiments, with technical assistance from S.W, with the exception of the first replicate of the 105 ms time point experiment, which was performed by S.W. M.C. performed the serial sectioning 3D reconstruction electron microscopy imaging and analysis. S.W. and M.C. developed MATLAB code for image analysis. K.P.A. and K.L. performed pilot zap-and-freeze experiments and electron microscopy sample preparation, imaging, and analysis. M.W.D. designed the prototype zap-and-freeze stimulation device. S.W. funded and oversaw the research.

References

71. Kaech, S. & Banker, G. Culturing hippocampal neurons. *Nat. Protoc.* **1,** 2406–2415

(2006).

72. Hoopmann, P., Rizzoli, S. O. & Betz, W. J. Imaging synaptic vesicle recycling by staining and destaining vesicles with FM dyes. *Cold Spring Harb. Protoc.* **7,** 77–83 (2012).

73. Hoppa, M. B., Gouzer, G., Armbruster, M. & Ryan, T. A. Control and plasticity of the presynaptic action potential waveform at small CNS nerve terminals. *Neuron* **84,** 778–789 (2014).

74. Watanabe, S. Flash-and-Freeze: Coordinating Optogenetic Stimulation with Rapid Freezing to Visualize Membrane Dynamics at Synapses with Millisecond Resolution. *Front. Synaptic Neurosci.* **8,** 24 (2016).

Figure Legends

Figure 1. Zap-and-freeze captures synaptic vesicle fusion. a, Schematic and photograph of the zap-and-freeze stimulation device. **b**, Epifluorescence micrographs of cultured mouse hippocampal neurons pre-incubated in 30 µM Pitstop 2 in physiological saline (1 mM Ca^{2+}) for 2 min, then either not stimulated or subjected to 10x 1 ms pulses at 20 Hz, at 37 °C in FM 1-43FX, followed by washing and fixation. Scale bar: 2 µm. **c**, Experimental design for stimulation and freezing, showing a diagrammatic excitatory postsynaptic potential for reference (based on [56]) . A 1-ms square pulse is applied to trigger a single action potential, then neurons are frozen 5 ms after the beginning of the pulse (this is the earliest possible freezing time on the high-pressure freezer, see Methods). **d-e**, Transmission electron micrographs of synapses from neurons high-pressure frozen in 1.2 mM Ca^{2+} either **d** without or **e** with tetrodotoxin (TTX), which prevents action potential firing. Samples were frozen either with no stimulation ("no stim") or 5 ms after stimulation, which presumably initiates an action potential ("5 ms after

AP"). The arrow indicates a pit in the active zone, which is presumed to be a synaptic vesicle fusing with the plasma membrane. The active zone is defined as the presynaptic plasma membrane opposite the post-synaptic density (PSD). Scale bar: 100 nm. Electron micrographs are from experiments described in Figure 3.

Figure 2. Multiple fusion events at single active zones after a single action potential.

a, Frequency distributions of number of fusion events 5 ms after an action potential (green) or without stimulation (grey) in solutions of 1.2, 2, or 4 mM Ca^{2+} (1.2 mM, no stim, n = 31; 1.2 mM, stim, n = 33; 2 mM, no stim, n = 34; 2 mM, stim, n = 36; 4 mM, no stim, n = 34; 4 mM, stim, n = 33 reconstructed active zones). Insets show the proportion, out of the active zones that contained at least 1 fusion event, that contained 1 fusion event (UVR, univesicular release) or more than 1 fusion event (MVR, multivesicular release). Fusion events are defined as "pits" in the active zone. Including all active zones from stimulated samples, number of pits was not significantly different in different Ca^{2+} concentrations ($p = 0.88$); including only synapses with at least 1 fusion event, there was significantly more fusion in 4 mM than in 1.2 mM ($p = 0.036$). The proportion of synapses that contained at least 1 pit was not different between samples stimulated in different Ca^{2+} concentrations ($p > 0.9$). **b,** Cumulative relative frequency distributions of locations of docked vesicles (with and without stimulation) and pits (after stimulation) within the active zone **(**n = 12, 20, 26 pits; 332, 467, 419 docked vesicles without stimulation; 234, 392, 245 docked vesicles with stimulation, ordered by increasing Ca^{2+} concentration). Locations are normalized to the size of the active zone and to the expected density of objects within a circular area by taking the square of the distance of a pit or vesicle to the center of the active zone divided by the half-length of the active zone: 0.25 would indicate a vesicle or pit halfway between the center and edge. Docked vesicles were not biased toward the

center or except for samples frozen in 4 mM Ca^{2+}, which were biased toward the center, and samples frozen after stimulation in 2 mM Ca^{2+}, which was biased toward the edge ($p > 0.7$ for each, except for 2 mM Ca^{2+} stim, $p = 0.01$; 4 mM Ca^{2+} no stim and stim, $p < 0.001$ for each). Vesicles fusions not biased toward the center or the edge ($p > 0.9$ for each). For each calcium concentration, the median location of pits and docked vesicles in the active zone after stimulation were similar to those of docked vesicles from no-stim controls ($p > 0.8$ for each). **c**, number of docked vesicles in each active zone reconstruction 5 ms after an action potential (green) or without stimulation (grey); same n as in **a.** The number of docked vesicles was not significantly different between synapses with and without pits for each calcium concentration ($p > 0.1$ for each comparison; Kruskal-Wallis test with post-hoc Dunn's multiple comparisons).. Vesicles that appeared to be in contact with the plasma membrane were considered docked. **d**, Width at base of pits in the active zone. Error bars indicate median and interquartile range. **e**, Cumulative relative frequency distributions of distances from center to center of pits and docked vesicles within the same active zone (n = 49 pairs of pits, 1057 pairs of docked vesicles; see Methods for description of distance calculation). Pit-to-pit distances were not significantly different from docked vesicle-to-docked vesicle distances ($p = 0.14$). Pairs of pits were from stimulated samples in 1.2, 2, and 4 mM Ca^{2+}; pairs of docked vesicles were from the no-stim 1.2 mM Ca^{2+} experiment. **f**, Same pit-to-pit distances in **e**, sorted by external calcium concentration. Scale bar: 100 nm. PSD: post-synaptic density. AP: action potential. Error bars in **c** indicate median and interquartile range. Each set of data is from a single experiment; experiments in 1.2 mM Ca^{2+} were performed on a separate day from a separate culture from the experiments in 2 mM and 4 mM Ca^{2+}. Number of pits and docked vesicles per active zone was compared using Kruskal-Wallis tests with post-hoc Dunn's multiple comparisons test. For pits, full pairwise comparisons were performed; for docked vesicles, only numbers of vesicles before and after stimulation at

each Ca^{2+} concentration were compared. Proportions of active zone reconstructions that contain at least one pit were compared using a chi-squared test. Bias of pit locations toward the center or edge of the active zone was tested by comparing each group to a theoretical median of 0.5, the expected median for a random distribution, using one-sample Wilcoxon signed-rank tests. Locations of pits, docked vesicles after stimulation, and docked vesicles without stimulation were compared using a Kruskal-Wallis test followed by post-hoc Dunn's test between pits and no-stim docked vesicles and stim docked vesicles and no-stim docked vesicles for each calcium concentration. P-values from all these pairwise and one-sample comparisons were adjusted with Bonferroni correction accounting for the total number of tests. The distributions of distances between pits in the same active zone and docked vesicles within the same active zone were compared using a Wilcoxon signed-rank test. See Extended Data Table 1 for full pairwise comparisons and summary statistics.

Figure 3. Vesicle fusion during the first 14 ms after an action potential.

a, Experimental design for stimulation and freezing, showing a diagrammatic excitatory postsynaptic potential for reference (based on [56]). A 1-ms square pulse is applied to trigger a single action potential, then neurons are frozen at the indicated time points after the beginning of the pulse. **b-f**, Example transmission electron micrographs of synapses from neurons frozen either **b** without stimulation, **c** 5 ms, **d** 8 ms, **e** 11 ms, or **f** 14 ms after stimulation. Arrows indicate pits in the active zone, which are presumed to synaptic vesicles fusing with the plasma membrane. **g**, Number of pits in the active zone per synaptic profile (part of the synapse captured in a 2-D section) in the above conditions, and without stimulation or 5 ms after stimulation in 1 μM tetrodotoxin (TTX, purple); (no stim, n = 274; 5 ms, n = 315; 8 ms, n = 343; 11 ms, n = 192; 14 ms, n = 211; TTX, no stim, n = 121; and TTX, 5 ms, n = 255 synaptic profiles**)**. Numbers of

pits with and without stimulation in TTX were not significantly different ($p > 0.9$). Numbers of pits at 14 ms and without stimulation were not significantly different ($p > 0.9$). **h**, Depth of pits within the active zone 5 ms (n = 65 pits), 8 ms (n = 66 pits), 11 ms (n = 17 pits), and 14 ms (n = 7 pits**)** after stimulation. the depth of pits at different time points were all similar ($p > 0.05$), except for 11 ms and 14 ms, which were significantly different from each other ($p = 0.002$). **i**, Location within the active zone of the same pits described in **h**. The pits at 11 ms were biased toward the center of the active zone ($p = 0.004$), while those at 5 ms and 8 ms were not biased toward the center or the edge ($p > 0.9$ in both cases). Scale bar: 100 nm. PSD: post-synaptic density. AP: action potential. Error bars in **g** indicate standard error of the mean; error bars in **h** and **i** indicate median and interquartile range. All data are from two experiments from separate cultures frozen on different days, except for the data from TTX treatment without stimulation, which are from a single experiment, and data from 5 and 8 ms, which are from three experiments. Numbers of pits in **g**, locations of pits in **h**, and heights of pits in **i** were compared using Kruskal-Wallis tests with full pairwise comparisons by post-hoc Dunn's multiple comparisons tests. Bias of pit locations toward the center or edge of the active zone was tested by comparing each group to a theoretical median of 0.5 using one-sample Wilcoxon signed-rank tests; Bonferroni correction was applied to all p-values from multiple-sample and one-sample tests to account for these extra comparisons. See Extended Data Table 1 for full pairwise comparisons and summary statistics.

Figure 4. Fusions captured at 5 and 11 ms after an action potential represent synchronous and asynchronous release. a-b, Example transmission electron micrographs of synapses from neurons pre-treated with **a** 0.25% DMSO or **b** 25 μM EGTA-AM and frozen either without stimulation, 5 ms after stimulation, or 11 ms after stimulation. Arrows indicate pits in the active

zone, which are presumed to be synaptic vesicles fusing with the plasma membrane. **c**, Number of pits in the active zone per synaptic profile (part of the synapse captured in a 2-D section) in the above conditions. p-values are from comparisons between EGTA- (no stim, n = 210; 5 ms, n = 209; 11 ms, n = 231 synaptic profiles) and DMSO-treated (no stim, n = 199; 5 ms, n = 241; 11 ms, n = 219 synaptic profiles) samples frozen at the same time point. Numbers of pits at 11 ms and without stimulation in EGTA-AM-treated samples were not significantly different ($p > 0.9$). **d**, Locations of pits within the active zone 5 ms (n = 39 pits) and 11 ms (n = 37 pits) after stimulation from neurons pre-treated with 0.25% DMSO. Pits at 11 ms were slightly but not statistically significantly biased toward the center of the active zone ($p = 0.059$), while those at 5 ms were not biased toward the center or the edge ($p > 0.9$). Scale bar: 100 nm. PSD: post-synaptic density. AP: action potential. Error bars in **c** indicate standard error of the mean. All data are from two experiments from separate cultures frozen on different days. Numbers of pits in **c** were compared using a Kruskal-Wallis test with full pairwise comparisons by post-hoc Dunn's multiple comparisons test (only comparisons between the same time point with and without EGTA-AM are shown). Locations of pits in **d** were compared using a Wilcoxon rank-sum test. Bias of pit locations toward the center or edge of the active zone was tested by comparing each group to a theoretical median of 0.5 using one-sample Wilcoxon signed-rank tests; Bonferroni correction was applied to all p-values from two-sample and one-sample tests to account for these extra comparisons. See Extended Data Table 1 for full pairwise comparisons summary statistics.

Figure 5. By 14 ms after an action potential, new docked vesicles have transiently replaced those that fused. a, Number of docked vesicles per synaptic profile (part of the synapse captured in a 2D section) from the same experiments and synaptic profiles as in Figure 3. Number of

docked vesicles at 14 ms was not significantly different from the no-stimulation control ($p > 0.9$). **b**, Same as **a**, except from the experiments in Figure 4. **c**, Distances of synaptic vesicles from the plasma membrane at the active zone, including both vesicles that were annotated as docked and not docked. Distances are binned in 2-nm increments, except for "0", which indicates vesicles ~0 nm from the active zone membrane ("2" indicates vesicles 0.1-2 nm from the membrane, "4" indicates 2-4 nm, etc.). The number of vesicles in the 0-2 nm range were significantly greater in the no-stim control than at all other time points but 14 ms. (0 nm: $p = 0.001$ for each pairwise comparison except to 14 ms, $p = > 0.9$; 0.1-2 nm: 5 ms, $p = 0.001$, 8 ms, $p = 0.007$, 11 ms, $p = 0.1$, 14 ms, $p > 0.9$; >98% of vesicles 0-2 nm from the membrane were annotated as docked). The only other multiplicity-corrected p-values less than 0.9 at any distance were for 14 ms ($p = 0.03$) at 6-8 nm and 11 ($p = 0.03$) and 14 ms (0.07) at 8-10 nm. **d**, Number of docked vesicles without stimulation or 105 ms after an action potential. Vesicles that appeared to be in contact with the plasma membrane were considered docked. Error bars indicate standard error of the mean. Numbers of docked vesicles in **a** and **b** were compared using a Kruskal-Wallis test with full pairwise comparisons by post-hoc Dunn's multiple comparisons test; Distances of synaptic vesicles from the active zone in the first 10 bins of data shown in **c** (0-18 nm from active zone) were compared to the no-stim control using a one-way ANOVA with post-hoc Dunnet's test, with all pairwise comparisons further multiplicity corrected using the method of Bonferroni to account for the 10 ANOVAs. The number of docked vesicles in **d** were compared using a Wilcoxon rank-sum test. Error bars represent standard error of the mean. See Extended Data Table 1 for full pairwise comparisons and summary statistics.

Extended Data Figure 1. Schematic of events at the active zone of a hippocampal bouton within the first 15 ms after an action potential. Synchronous fusion, often of multiple vesicles,

begins throughout the active zone within hundreds of microseconds, and the vesicles finish collapsing into the plasma membrane by 11 ms (note that the high local calcium shown only lasts ~100 microseconds). Between 5 and 11 ms, residual calcium triggers asynchronous fusion, preferentially toward the center of the active zone. Although shown here as taking place in the same active zone, the degree to which synchronous and asynchronous release may occur at the same active zone after a single action potential is unknown. By 14 ms, the vesicles from the peak of asynchronous fusion, which can continue for tens to hundreds of milliseconds, have fully collapsed into the plasma membrane, and new docked vesicles, which may start to be recruited in less than 10 ms, have fully replace the vesicles used for fusion. These vesicles then undock or fuse within 100 ms. Whether these new vesicles dock at the same sites vacated by the fused vesicles, and whether newly docked vesicles contributed to synchronous and asynchronous fusion during the first 11 ms, remains to be tested.

Extended Data Figure 2. Multiple fusion events in serial-sectioning reconstructions of active zones from neurons frozen 5 ms after an action potential. a, Example transmission electron micrographs from serial sections of active zones from neurons frozen 5 ms after an action potential in 1.2 mM, 2 mM, and 4 mM extracellular Ca^{2+} (from the same experiments described in Figure 2). Scale bar: 100 nm. PSD: post-synaptic density. AP: action potential. Arrows indicate "pits" in the active zone (opposite the post-synaptic density), which are presumed to be vesicles fusing with the plasma membrane. Note that pits within the same active zone are often different heights.

Extended Data Figure 3. Representations of serial-sectioning reconstructions of active zones with exocytic pits. Graphical depictions of all serial-sectioned active zones containing

exocytic pits, from the experiments described in Figure 2. Each horizontal line represents the length of a single synaptic profile, with each stack representing a serial-sectioned active zone. Open circles represent docked vesicles; notches represent pits in the active zone.

Extended Data Figure 4. Fusion intermediates at multiple time points during the first 14 ms after an action potential. a-b, Example transmission electron micrographs of synapses from neurons frozen without stimulation or 5, 8, 11, or 14 ms after an action potential (these are other examples from the same experiments shown in Figure 3). **c**, Cumulative relative frequency of locations of docked vesicles within the active zone, normalized to the size of the active zone (no stim, n = 447; 5 ms, n = 300; 8 ms, n = 348; 11 ms, n = 188; 14 ms, n = 306 docked vesicles). **d**, Same data as in **c**, showing only vesicles from synaptic profiles that contain pits. **e**, Same data as in **c**, showing only vesicles from synaptic profiles that contain do not contain pits. Note that distributions of docked vesicle locations are qualitatively similar to those of pit locations at 5 ms in Figure 3 and Figure 4. Scale bar: 100 nm. PSD: post-synaptic density. AP: action potential. Arrows indicate "pits" in the active zone (opposite the post-synaptic density), which are presumed to be vesicles fusing with the plasma membrane. See Extended Data Table 1 for full pairwise comparisons and summary statistics.

Extended Data Figure 5. Chelating residual Ca^{2+} blocks fusion intermediates at 11 ms but not 5 ms after an action potential. a-b, Example transmission electron micrographs of synapses from neurons pre-treated with **a** 0.25% DMSO or **b** 25 μM EGTA-AM and frozen either without stimulation, 5 ms after stimulation, or 11 ms after stimulation (these are other examples from the same experiments shown in Figure 4). Scale bar: 100 nm. PSD: post-synaptic density. AP: action

potential. Arrows indicate “pits” in the active zone (opposite the post-synaptic density), which are presumed to be vesicles fusing with the plasma membrane.

Figure 1, Kusick et al.

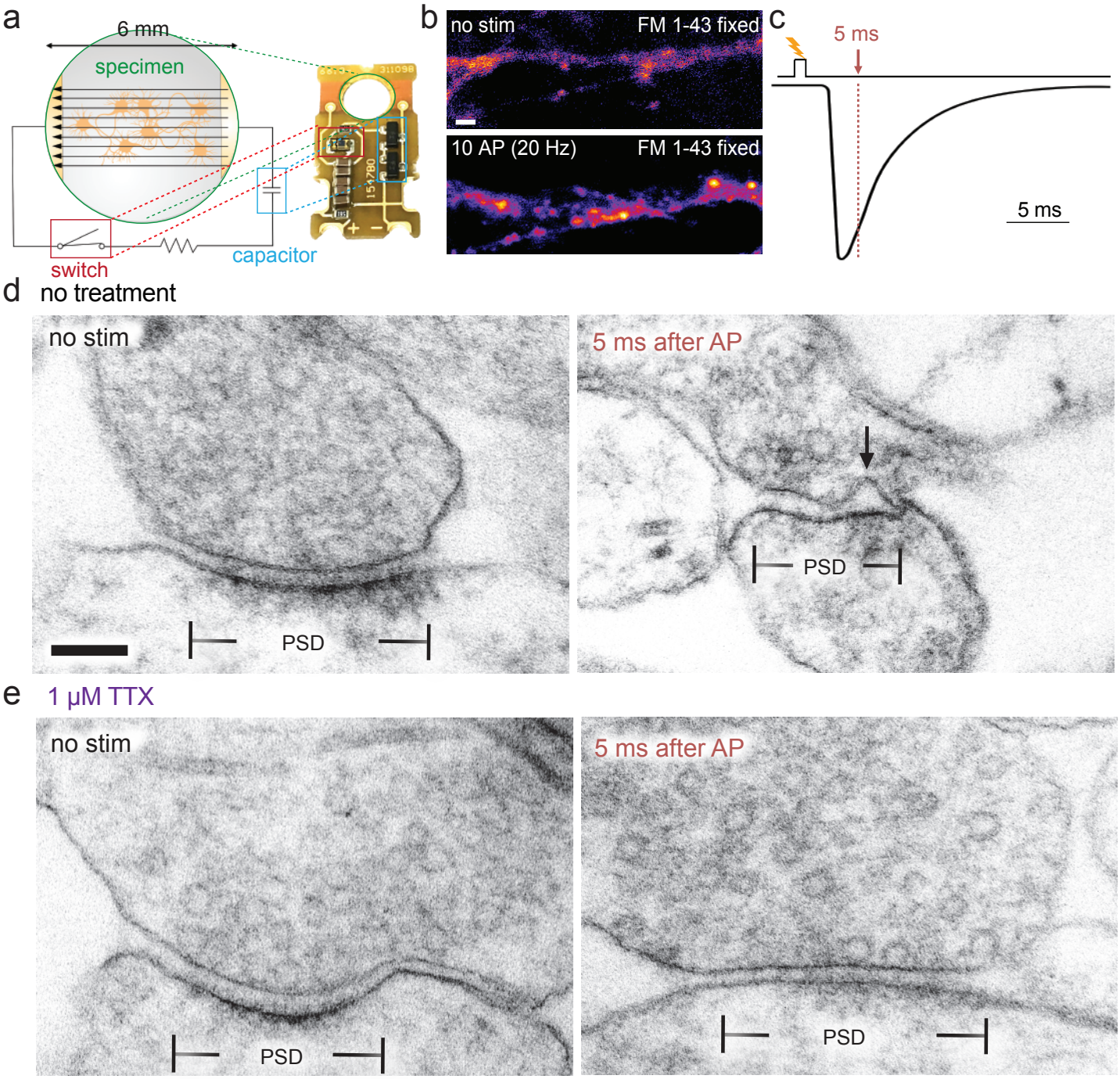

Figure 2, Kusick et al.

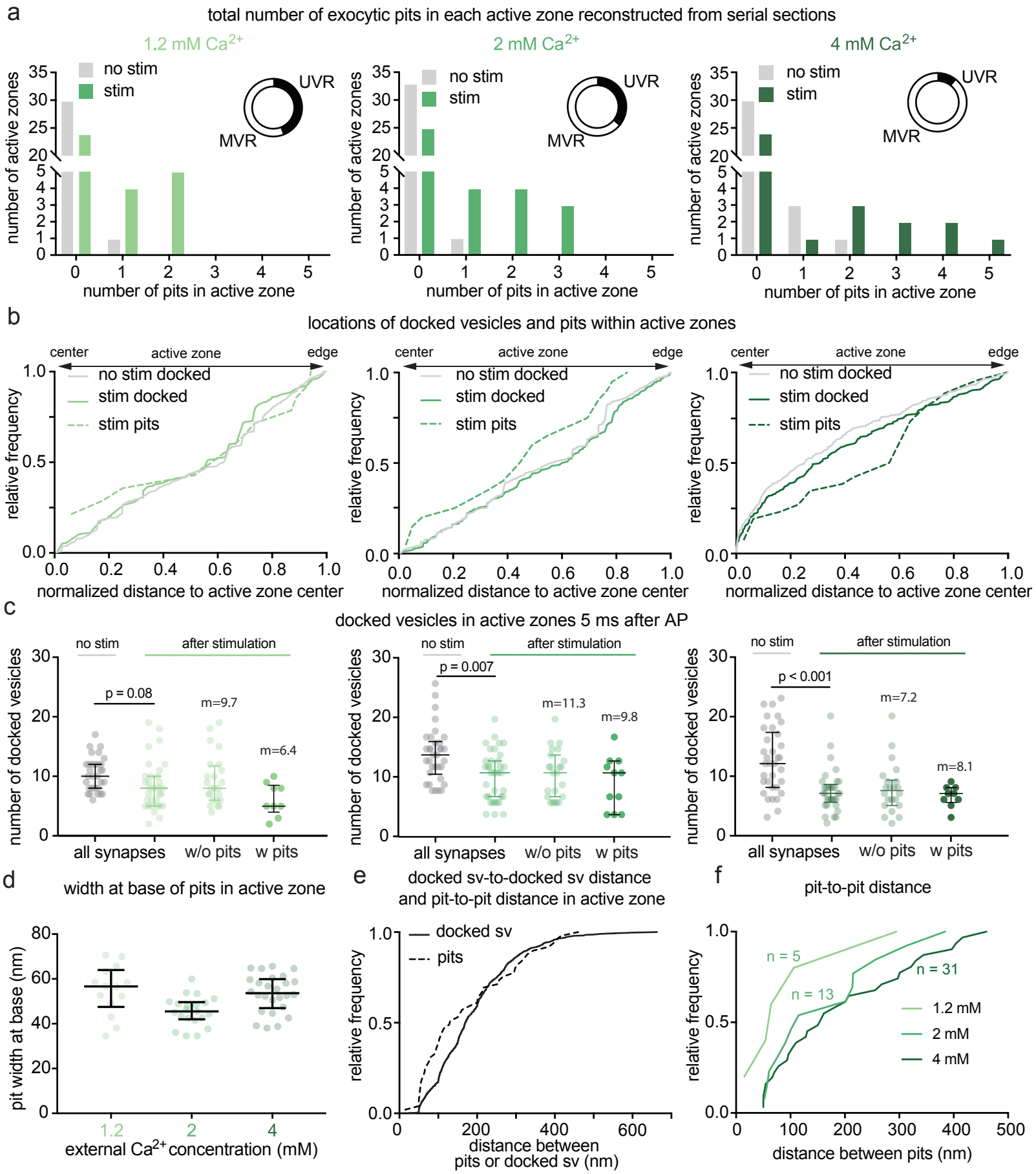

Figure 3, Kusick et al.

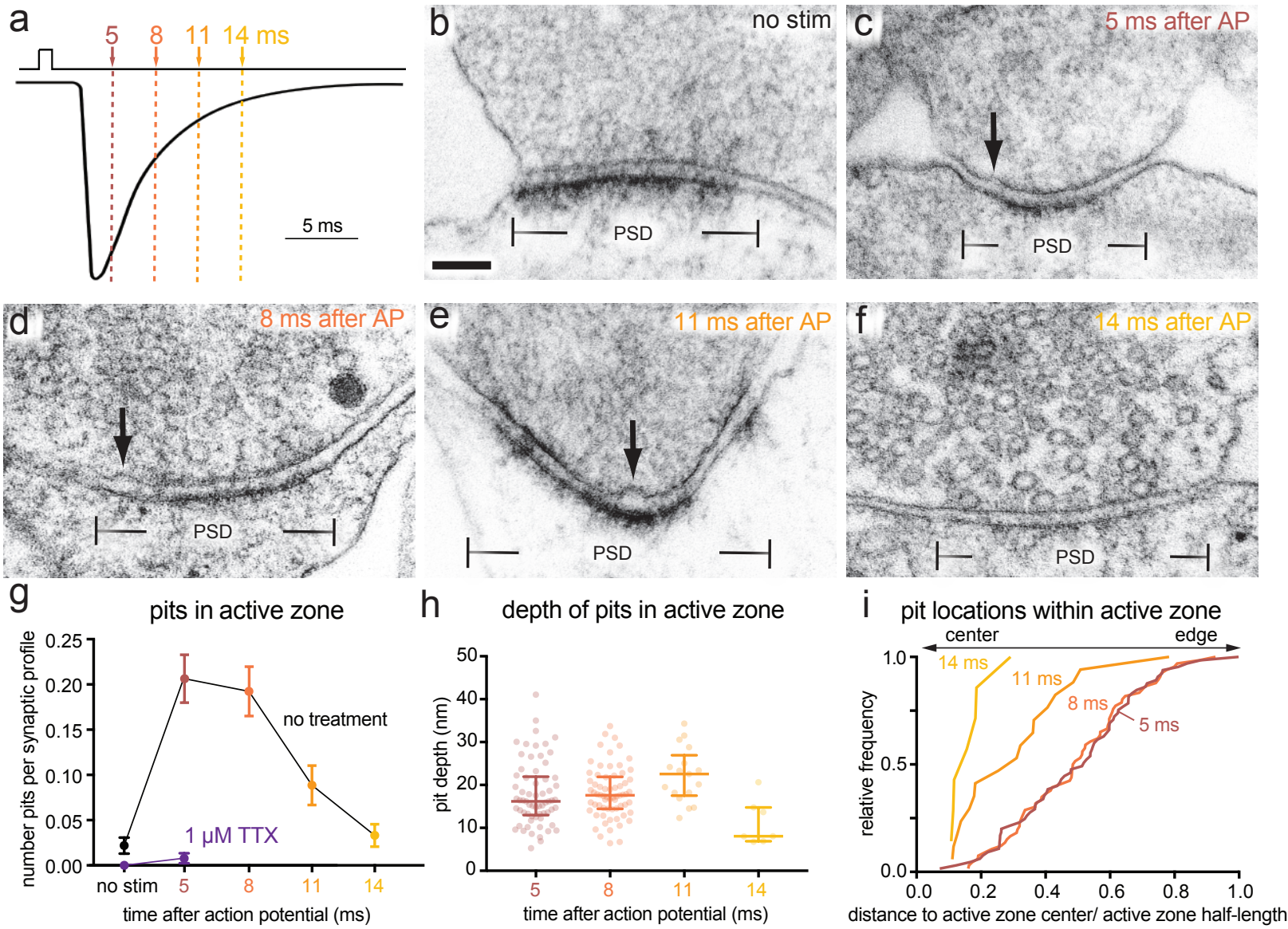

Figure 4, Kusick et al.

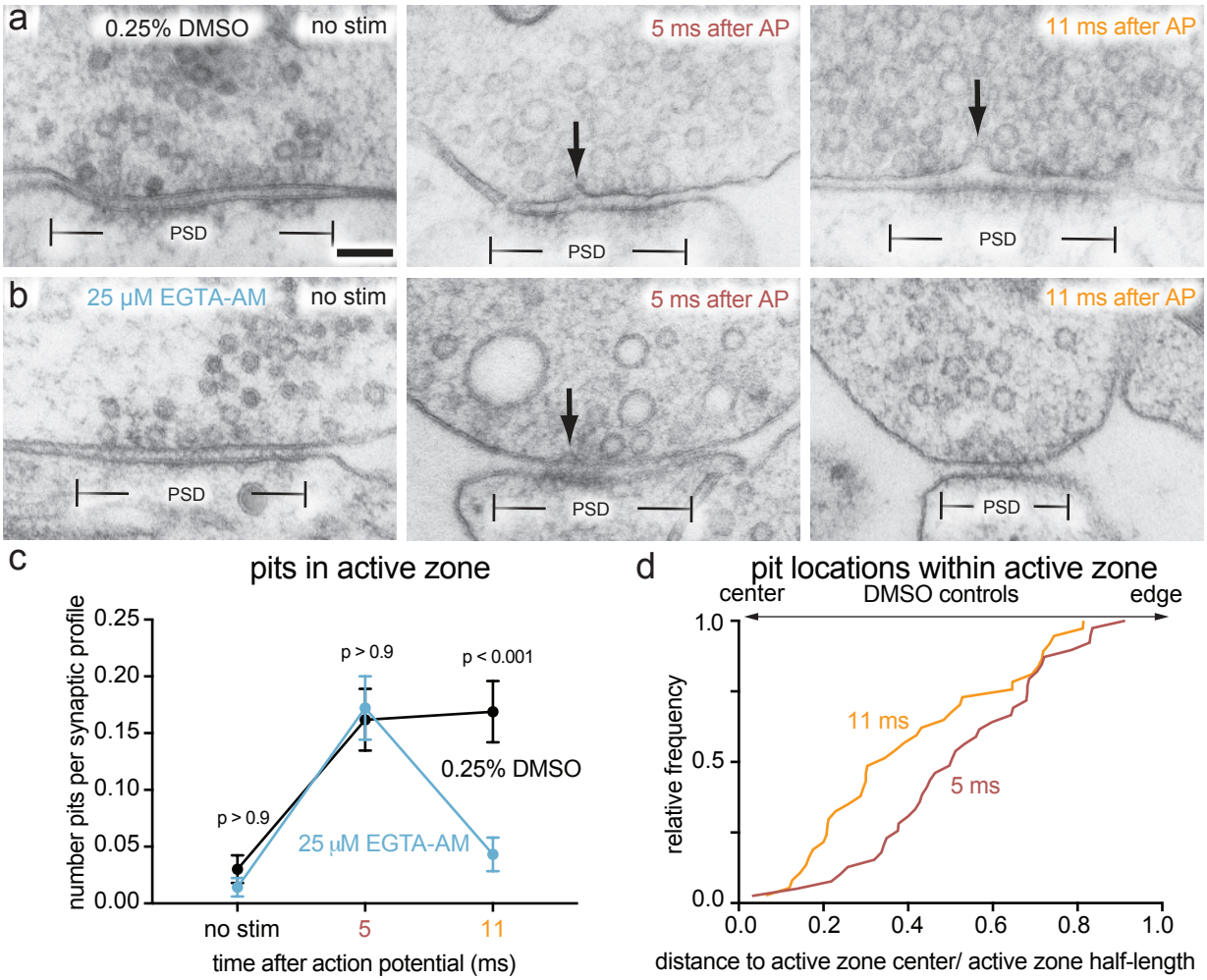
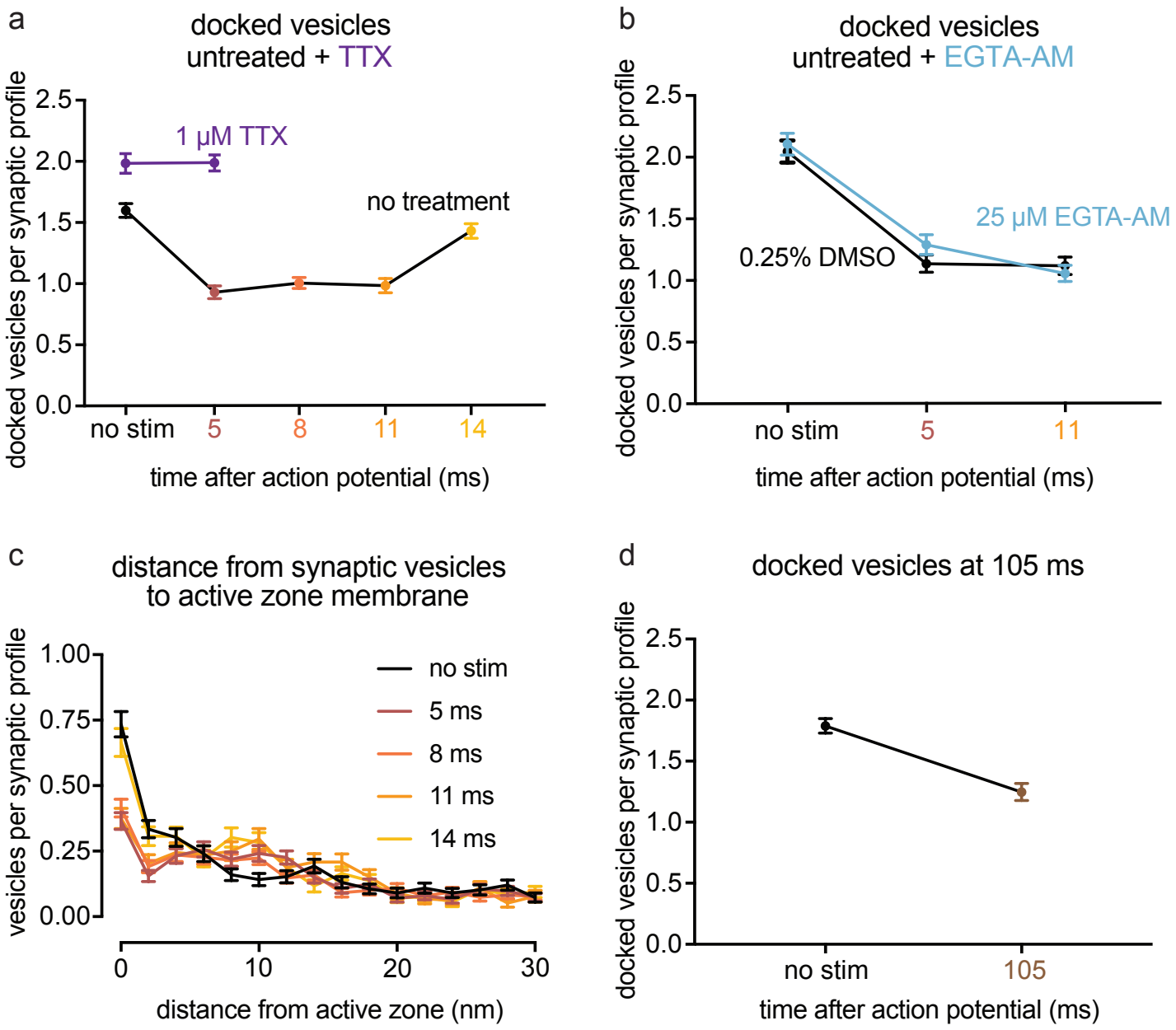
Figure 5, Kusick et al.